

# Temperature-Emissivity Separation with ASTER and LANDSAT 7 Validation on the fringe of the Okavango Delta, Botswana

Ambro S. Gieske<sup>\*a</sup>, Michael T. Wubett<sup>a</sup>, Wim J. Timmermans<sup>a</sup>, Gabriel N. Parodi<sup>a</sup>,  
Piotr Wolski<sup>b</sup>, Almuth Arneth<sup>c</sup>

<sup>a</sup>ITC, International Institute for Geo-Information Science and Earth Observation, P.O. Box 6,  
7500 AA Enschede, The Netherlands

<sup>b</sup>Harry Oppenheimer Okavango Research Centre, Private Bag 285, Maun, Botswana

<sup>c</sup>Max Planck Institute for Biogeochemistry, Carl-Zeiss Promenade 10, 07745 Jena, Germany

## ABSTRACT

Land surface temperatures are important in global change studies, in estimating radiation budget, heat balance studies and as control for climate models. Several algorithms for estimating land surface temperature and emissivity spectra for multispectral thermal infrared images were developed recently for use with data from the Advanced Spaceborne Thermal Emission and Reflection Radiometer (ASTER) on the TERRA platform. Similar methods are also used with the MODIS instrument.

In this study, surface temperature and broadband emissivities were determined from the five TIR channels of ASTER instrument in an area on the southern fringe of the Okavango Delta (Botswana). MODTRAN 4 was used to determine the necessary atmospheric corrections while software was developed to facilitate MODTRAN post-processing. The results were compared with micrometeorological observations from a flux tower, with a LANDSAT 7 image of the same day, and finally also with reported ASTER surface temperature and emissivities for the same image (high level ASTER product).

Results indicate that the surface temperature depends rather sensitively on atmospheric transmissivity and relatively large temperature differences are found between results from imagery analysis and flux tower. No relation was found between broad-band emissivity and NDVI, contrary to earlier findings in Botswana.

**Keywords:** ASTER, LANDSAT, temperature-emissivity separation, land surface temperature, Okavango, Botswana

## 1. INTRODUCTION

Energy balance methods for the determination of evapotranspiration by remote sensing techniques<sup>1,2,3</sup> depend on information both from the visible and TIR domain. Determination of the reflection coefficients in the visible part of the spectrum makes it possible to determine net short wave energy, while information on plant growth is obtained through the NDVI index. The thermal images allow evaluation of the surface temperature, emissivities and net long wave energy. The values of the basic input parameters NDVI, Albedo and surface temperature are highly influenced by the atmospheric conditions at the time of satellite overpass and it is therefore important to assess the influence of atmospheric correction methods on the parameter values. Here we restrict ourselves to a study of surface temperature. However, it should be borne in mind that the main objective of our study is to develop energy balance algorithms in semi-arid terrain with standard satellites and a minimum of ancillary meteorological information. For example, the SEBAL energy balance method<sup>2</sup> derives broad-band emissivity from the NDVI parameter, it does not apply any

---

\* [gieske@itc.nl](mailto:gieske@itc.nl); phone 0031-53-4874498; fax 0031-53-4874336

atmospheric correction in the TIR bands and therefore produces results that are substantially different from those obtained by methods that make atmospheric corrections. Despite this the SEBAL method produces good results because it depends more on temperature differences in the scene than on the absolute value of the temperature.

In this paper a series of ASTER and LANDSAT Thermal Infrared (TIR) images is studied in an area on the southern fringe of the Okavango Delta (Maun, Botswana). Ground truth is supplied by a flux tower (a joint project of HOORC and Max Planck to study fluxes above a Mophane forest), which has been operational from 1999 onwards<sup>4,5</sup>. The area (Fig. 1) is situated a few km from the Thamalakane River which marks the southwestern boundary of the Okavango Delta which is a protected RAMSAR wetland site. Annual floods arrive in Maun in July in the dry season as a result of rainfall in Angola, 7 months earlier. Thus large parts of the Delta are flooded perennially even in the dry season. Immediately outside the Delta area however, much more arid conditions prevail as the annual rainfall is only 500 mm. In the case of the ASTER imagery the atmospheric parameters  $\tau_j$ ,  $L_j^\uparrow$  and  $L_j^\downarrow$  are usually determined with the MODTRAN path radiance code<sup>8,9,22</sup>, provided suitable atmospheric sounding data is available with respect to aerosols, water vapour, ozone, temperature and pressure.

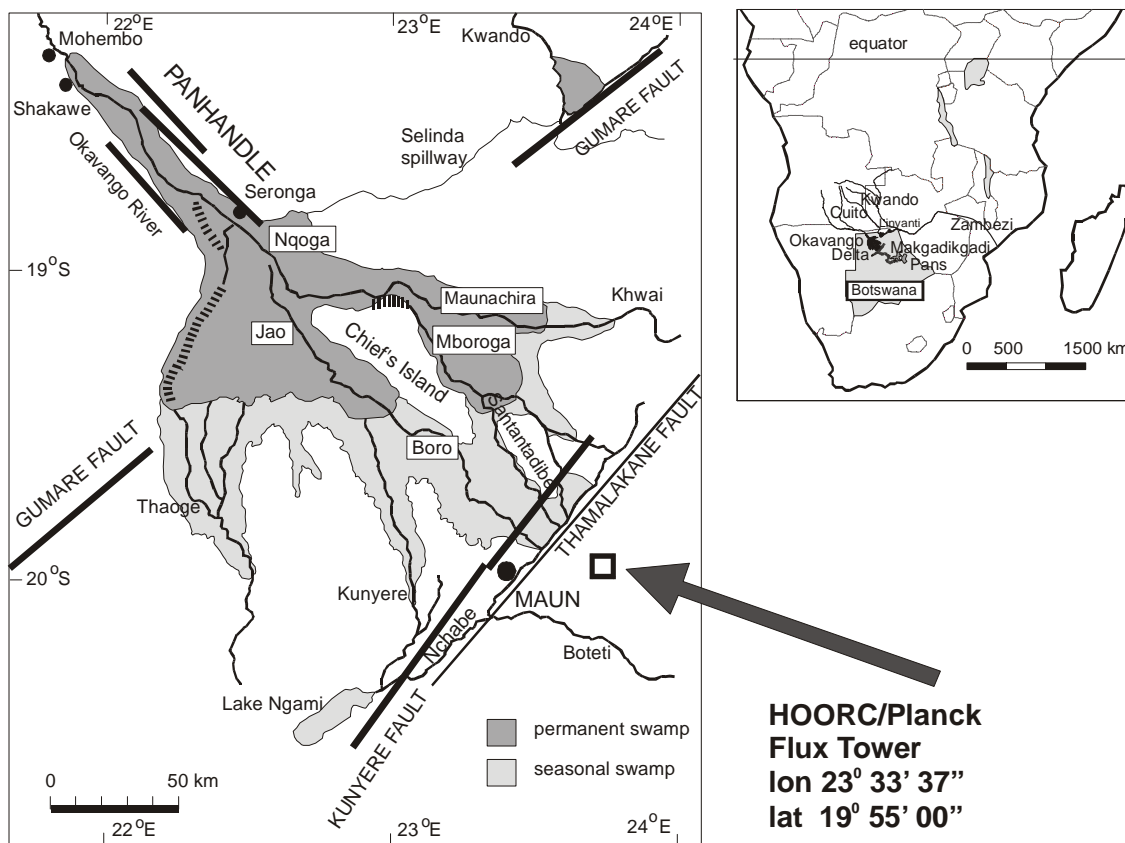


Fig.1. Location map of study area, showing Botswana, the Okavango Delta and the position of the micrometeorological flux tower.

Extensive ground truth and imagery are available from ongoing research work in the area through projects as for example, SAFARI2000 and through ongoing research from the Harry Oppenheimer Okavango Research Centre (University of Botswana). The flux tower was established to study sensible heat, evaporative and carbon dioxide fluxes above a Mopane forest. It is equipped with eddy correlation instruments and a range of standard meteorological instruments, including sensors for short and long wave incoming and outgoing radiation at 12 m height, with a forest canopy of about 5 m around the station. Furthermore, there are a number of soil heat flux plates and subsurface temperature sensors attached to the station. The radiation sensors are of specific interest to this paper.

In Section 2 a summary is given of the theory with respect to conversion of radiances to temperature, with temperature-emissivity separation as the most advanced method. MODTRAN/LOWTRAN type models are commonly used for atmospheric correction in the thermal infrared. Section 3 discusses the dataset of the flux tower, the available images ASTER and LANDSAT imagery and the preprocessing required. The results are presented in Section 4, while finally conclusions are given in Section 5.

## 2. TES ALGORITHM AND ATMOSPHERIC CORRECTION

The spectral radiance of a black body at temperature T is given by the Planck function<sup>6</sup>

$$L_j^{BB} = \frac{C_1}{\lambda_j^5 \pi \left[ \exp\left(\frac{C_2}{\lambda_j T}\right) - 1 \right]} \quad (1)$$

where

$$\begin{aligned} L_j^{BB} &= \text{black body radiance (Wm}^{-2}\mu\text{m}^{-1}\text{sr}^{-1}) \\ \lambda_j &= \text{wave length of channel } j \text{ (}\mu\text{m)} \\ T &= \text{temperature of black body (K)} \\ C_1 &= 3.74177492 \times 10^8 \text{ (Wm}^{-2}\mu\text{m}^4\text{sr}^{-1}) \\ C_2 &= 1.43876912 \times 10^4 \text{ (}\mu\text{mK)} \end{aligned}$$

Most surface materials emit less radiation at a certain temperature than a black body at the same temperature, i.e. radiation  $L_j^{surf}$  depends on the surface emissivity  $\epsilon_j$  through

$$L_j^{surf} = \epsilon_j L_j^{BB} \quad (2)$$

The radiances measured at the satellite  $L_j^{sat}$  are further modified through atmospheric effects as<sup>7</sup>

$$L_j^{sat} = L_j^{surf} \tau_j + L_j^\uparrow \quad (3)$$

where  $\tau_j$  is the atmospheric transmissivity and  $L_j^\uparrow$  the radiance upwelling from the atmosphere. Finally, also the downwelling atmospheric radiance  $L_j^\downarrow$  has to be taken into account, and this leads, in combination with Eqns 1 and 2, to the expression

$$L_j^{sat} = \left[ \epsilon_j L_j^{BB} + (1 - \epsilon_j) L_j^\downarrow \right] \tau_j + L_j^\uparrow \quad (4)$$

The final problem is then to determine the emissivities for each band together with one surface temperature channel. The ASTER imagery has 5 TIR bands (10-14), so through the use of Eqn (4) 5 equations are found. However, there are 6 unknowns: 5 emissivities and one temperature T. One additional relation is required to solve the system of equations.<sup>10,11</sup> reviewed a number of the older methods, while another method was proposed recently<sup>12</sup>. Here the TES method<sup>7,13</sup> is used which makes use of the max-min (MMD) differences between the relative maximum and minimum emissivities  $\beta_j$ .

$$\beta_j = \frac{L_j / L_j^{BB}(T)}{L / L_j^{BB}(T)} \quad (5)$$

where L is the average radiance of all channels<sup>8</sup>. From laboratory measurements the relationship between  $\epsilon_{min}$  and MMD is given as

$$\epsilon_{\min} = 0.994 - 0.687xMMD^{0.737} \quad (6)$$

This value for  $\epsilon_{\min}$  can be used to calculate new emissivity values as

$$\epsilon_j = \beta_j \left( \frac{\epsilon_{\min}}{\min(\beta_j)} \right) \quad (7)$$

From these emissivities a new temperature can be obtained. The process is repeated until the results converge which is after two to three iterations usually.

The band emissivities can be combined into a broadband emissivity in the atmospheric window from 8-12  $\mu\text{m}$  according to several methods<sup>14,15,16</sup>. Here we use<sup>14</sup>

$$\epsilon_{8-12} = \sum_{j=10}^{14} a_j \epsilon_j + c \quad (8)$$

where coefficients  $a_j$  and  $c$  are given by<sup>14</sup>. Finally, we assume here that the relation between radiant surface temperature  $T_{\text{rad}}$  and kinetic surface temperature  $T_{\text{kin}}$  is given by<sup>17</sup>

$$T_{\text{rad}} = (\epsilon_{8-12})^{1/4} T_{\text{kin}} \quad (9)$$

Furthermore, a number of authors<sup>18,19</sup> have discussed a simplified procedure for LANDSAT which has a single thermal band (band 6 from 10.5-12.5  $\mu\text{m}$ ). The first approximation is that the downwelling radiance  $L_{\downarrow}$  can in practice be taken as equal to the upwelling radiance  $L_{\uparrow}$ . The upwelling radiance is then related to the atmospheric temperature at 2m elevation through simple relations where the coefficients are determined through the use of LOWTRAN. The atmospheric transmissivity is found from the total atmospheric water vapor content through a set of temperature dependent linear relations. However, the surface emissivity has to be supplied independently.

Finally,<sup>17</sup> and<sup>20</sup> discussed terminology and conceptual problems in thermal infrared remote sensing of natural surfaces. Directional dependence of radiance and surface temperature<sup>21</sup> will not be discussed in this paper.

### 3. IMAGE PROCESSING AND FLUX TOWER DATA

Searching the ASTER database for suitable level 1B images, covering the area around the flux tower yielded two dates: February 2002 and August/September 2000. Unfortunately no flux tower data were available for February 2000. However, for August 25 both ASTER 1B and LANDSAT 7 ETM+ images were archived, and validated flux tower data were also available for that period. Further search yielded suitable ASTER level 1A images on July 8, 2000, November 13, 2000 and January 7, 2001. The image dates are summarized in Table 1, which also shows the recorded data at the time of the satellite overpasses. Fig. 2 shows the air temperature and rainfall in the area for the period July 1, 2000 until January 31, 2001. The figure shows the abrupt change from winter in Botswana (July) to summer temperatures, which are reached by the end of September. Some rain fell in the period from September 26 to November 13, 2000.

The ASTER 1A and 1B images were processed for radiometric calibration and geometric correction in accordance with the information in the HDF files<sup>23</sup>. Similar procedures were followed for the L7 ETM+ image. The geometric correction was then stepwise improved with ground truth GPS track and waypoint data, and all ASTER images were then tied in to the L7 image coordinate system.

**Table 1** Summary of the Flux Tower data recorded at the time of satellite overpasses.

	ASTER 1A	ASTER 1B	ASTER 1B	ASTER 1A	ASTER 1A	ETM+
	8-Jul	25-Aug	26-Sep	13-Nov	7-Jan	25-AugL7
Julian day	189	237	269	317	7	237
day since July 1, 2000	8	56	88	136	191	56
loctime overpass (UTC+2)	10.9679	10.9624	10.9537	10.9353	11.0220	10.2736
p (mbar)	918.71	915.22	909.08	905.93	906.00	915.56
air T (7m elev) (C)	17.32	23.47	30.40	27.36	31.61	21.88
RH (%)	49.74	25.02	15.77	18.01	25.45	28.77
density $\rho$ ( $\text{gm}^{-3}$ )	1097.33	1071.62	1040.29	1047.31	1030.50	1077.67
wind horizontal ( $\text{ms}^{-1}$ )	4.42	4.48	2.29	3.49	2.11	4.73
ShortWDownRad ( $\text{Wm}^{-2}$ )	653.52	767.17	897.37	1029.52	1016.41	669.25
ShortWUpRad ( $\text{Wm}^{-2}$ )	88.75	114.24	151.08	157.81	142.46	101.20
Albedo (%)	13.58	14.89	16.84	15.33	14.02	15.13
LongWDownRad ( $\text{Wm}^{-2}$ )	352.18	378.54	437.97	378.31	421.15	366.37
LongWUpRad ( $\text{Wm}^{-2}$ )	422.83	471.73	556.33	533.47	547.65	453.33
Trad (C)	20.70	28.84	41.56	38.28	40.33	25.85
PAR ( $\mu\text{mols}^{-1}\text{m}^{-2}$ )	1200.33	1396.55	1657.94	1884.88	1889.78	1208.49
Rn ( $\text{Wm}^{-2}$ )	494.12	559.74	627.92	716.55	747.44	481.09
SoilHeatFlux ( $\text{Wm}^{-2}$ )	84.77	100.52	146.66	197.86	197.89	85.63
SoilTemp_2cm (C)	19.38	28.05	37.50	42.07	43.30	24.36
SoilTemp_5cm (C)	16.42	22.34	29.50	33.11	34.15	20.06
SoilTemp_10cm (C)	14.86	19.72	26.09	29.27	29.74	18.79
SoilTemp_50cm (C)	19.13	22.12	26.17	29.80	29.83	22.15
SoilTemp_100cm (C)	21.06	22.40	25.32	28.64	28.95	22.40

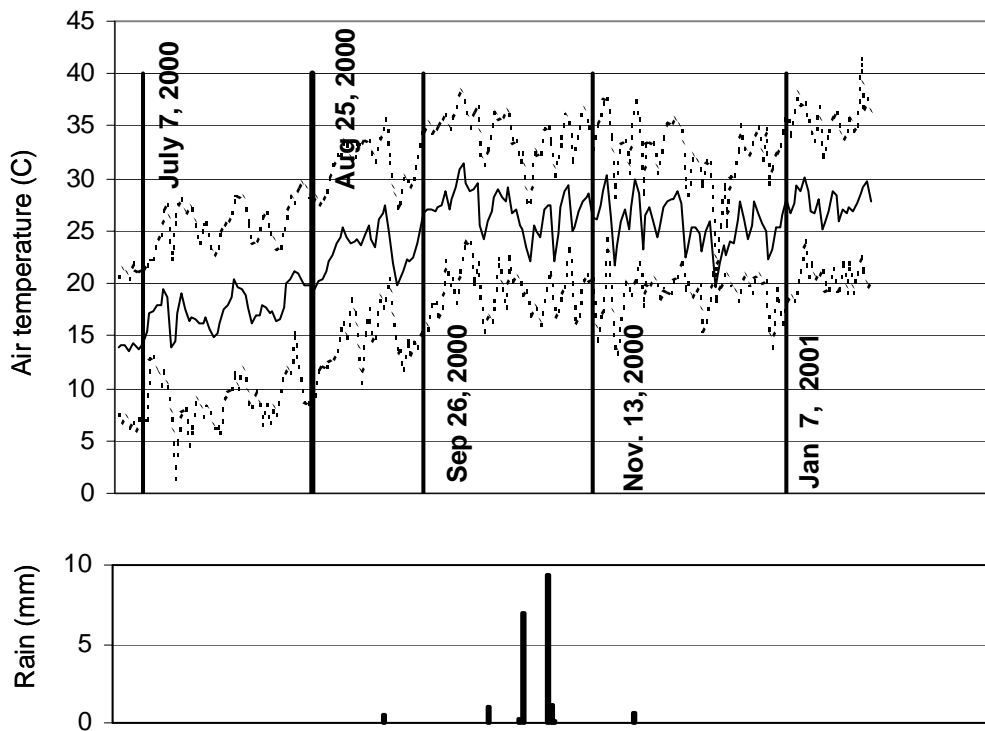


**Figure 2.** Air temperature (daily average, maximum minimum) and rainfall recorded by the Flux Tower in the period from July 1, 2000 - January 31, 2001.

## 4. RESULTS

The flux tower's surface temperatures are shown in Table 2, based on  $L_{\downarrow}$  and  $L_{\uparrow}$ . There is a clear increase from July to January from winter to summer. Three methods may be used to determine temperatures (a) this method does not use emissivity and determines in fact a brightness temperature. These temperatures are given in the Flux Tower's records. Method (b) makes use of both the emissivity and the fraction of the downward long wave radiation that is not absorbed  $(1-\epsilon)L_{\downarrow}$ . Here it is considered that  $L_{\downarrow}$  may measure the surface leaving radiance. Finally (c) is calculated using  $\epsilon\sigma T_0^4$ . The table shows that the last line of the table (option c) gives the highest surface temperatures. One should interpret the emissivity and temperature as a compound property of both soil and canopy in the field-of-vision of the tower's downward looking long wave sensor. As a result from the ASTER analysis (see below) an emissivity value of 0.92 was taken in the calculations.

**Table 2** Surface temperatures derived from the flux tower's long wave sensors.

	$\epsilon=0.92$	ASTER	ASTER	ASTER	ASTER	ASTER	LANDSAT
		7-Jul	25-Aug	26-Sep	13-Nov	7-Jan	25-Aug
$L_{\text{down}} \text{ (Wm}^{-2}\text{)}$		352.18	378.54	437.97	378.31	421.15	366.37
$L_{\text{up}} \text{ (Wm}^{-2}\text{)}$		422.83	471.73	556.33	533.47	547.65	453.33
$T_{\text{rad}} \text{ (C)}$	$L_{\text{up}}=\sigma T_{\text{rad}}^4$	20.70	28.84	41.56	38.28	40.33	25.85
$T_{\text{surf}} \text{ (C)}$	$L_{\text{up}}=\epsilon\sigma T_{\text{surf}}^4-(1-\epsilon)L_{\text{down}}$	21.78	30.15	43.03	40.25	41.91	27.12
$T_0 \text{ (C)}$	$L_{\text{up}}=\epsilon\sigma T_0^4$	26.90	35.23	48.21	44.86	46.95	32.17

The results of the ASTER image analysis are summarized in Table 3. First, the ASTER products AST08 and AST05 are provided with the level 1B images, and give surface kinetic temperatures and narrow-band emissivities respectively. The narrow band values were converted to a broad-band value (8-12  $\mu\text{m}$ )<sup>14</sup>. The pixel values around the tower site were inspected after careful geometric correction. However, since the area around the flux tower is rather homogeneous, the values of neighbouring pixels are rather close to the value recorded in the Table 3. The emissivity values are lower than what one would normally expect from a forest canopy. However, the Mopane canopy is sparse in the vicinity of the tower and moreover, the Mopane leaves are fairly brown most of the year. The second and third groups show the results of calculations with MODTRAN 4 followed by TES calculations<sup>13</sup>, with programs implemented by the authors. Two standard model atmospheres were used: Midlatitude winter (45N) and the US 1976 standard atmospheres. Furthermore, it was necessary to process the 1A images for the necessary radiometric corrections, using coefficients embedded in the

**Table 3** Emissivities and surface temperatures derived from ASTER images

ASTER Processing		1A	1B	1B	1A	1A
		8-Jul	25-Aug	26-Sep	13-Nov	7-Jan
		189	237	267	317	372
		8	56	88	136	191
Products	$\epsilon_{8-12}$		0.920	0.914		
(AST05 and AST08)	t (C)		36.85	51.20		
MidLat Winter	$\epsilon_{8-12}$	0.946	0.935	0.925	0.928	
	t (C)	27.05	36.80	50.28	49.76	
US1976	$\epsilon_{8-12}$			0.923	0.923	0.929
	t (C)			51.30	50.86	47.60

HDF image files. The results surprisingly show that the image derived temperature values are systematically higher than those resulting from the flux tower. Figure 3 shows this in a scatter plot. The slope is 1.08, giving a difference of 1.6 C at 20 C and a difference of 3.2 C on average for surface temperatures of around 40 C. One would expect the image

temperatures to be lower, because the tower's long wave sensor is looking down on fairly sparse canopy as mentioned above. Although one cannot a priori completely rule out sensor problems, this does not appear likely at present.

For the LANDSAT7 ETM+ image of 25 Aug. 2000 a mono-window correction algorithm was used<sup>18</sup>. With a transmissivity of 0.85 and an emissivity value of 0.93 (Band 6 value) a temperature of 36.75 C was found. The value for the transmissivity value in this method depends on the total atmospheric water vapour content. Analysis of the NVAP Langley database for 1999 showed that there are significant daily fluctuations in the Maun area over the year. Unfortunately no values of total water vapour for 2000 were available to us at the time of investigation. Ordinary processing<sup>2</sup> according to the relation  $L_{sat} = \epsilon \sigma T_0^4$  yielded a temperature of 33.7 C. These values were also plotted in Figure 3, and remarkably also fitted the regression line rather well.

Finally, several authors have proposed to estimate broadband emissivity from NDVI values. For example, in southeastern Botswana the relation  $\epsilon_0 = 1.0094 + 0.047 \ln(\text{NDVI})$  was established<sup>24</sup>. The relation is used in energy balance calculations<sup>2</sup> as a quick way of determining surface temperature from at-satellite radiance. It is therefore important to see how this relation performs in the Okavango/Maun environment in comparison to the TES techniques. The LANDSAT7 ETM+ image of August 25, 2000 was processed to produce NDVI and emissivity maps using the linear relation above. Emissivity values from the ASTER product AST05 can be used in a straightforward manner.

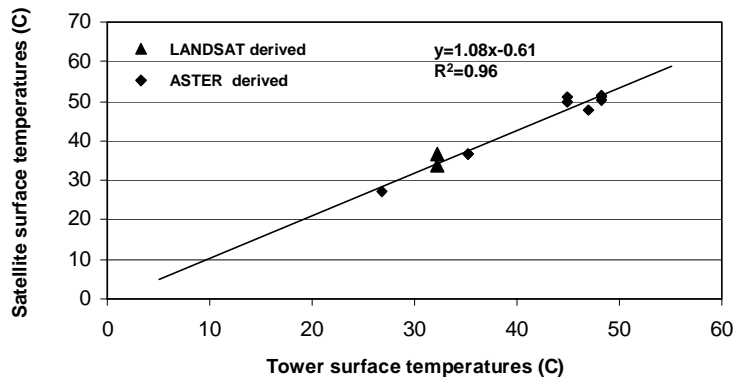


**Figure 3** Surface temperatures derived from the satellite analysis plotted against the temperatures derived from the flux tower's long wave sensors.

After careful geocorrection and resampling to 90 m resolution, the pixel values of both maps can be plotted in a scatter diagram. Because of the large number of points to be compared (in the order of 700x700) a large random subset was taken from the images to produce the diagram of Fig. 4. It is obvious that the correlation between the two methods is rather poor. The figure also shows that the ASTER derived emissivity distribution is bimodal, i.e. there is a distinct group of high emissivity values. In the images these values correspond to the flooded parts of the Okavango. It should be noted that the climate in Botswana is generally very dry in the winter months from April to October, but that the floods arrive in Maun in July after a long journey from Angola through the upper parts of the Delta. Thus there is a plausible explanation for the bimodal distribution, which is probably caused by the contrast between the flooded area with abundant vegetation and the desert and savanna like landscape surrounding it. It is remarkable, however, that the emissivity derived from the NDVI's does not show such a bimodal pattern.

The overall low correlation between the results of the two methods to determine emissivity also leads to large temperature differences, and low correlation between temperature maps. The energy balance calculations are therefore affected and care should be taken when comparing results of different methods<sup>1,2,3</sup>.

## 5. DISCUSSION

Two issues were raised in this paper:

1. The relation between surface kinetic temperatures derived from satellite images and the temperatures determined from ground truth.
2. The general value of empirical emissivity-NDVI relations

With regard to the first issue, satellite images “see” an integrated mixture of surface elements due to their low TIR resolution. So especially in the present case where a sparse, but broad-leaved, Mopane forest on white sandy soils was studied, many remote sensing complications arise. The calculations have shown that there is a clear linear relation between the satellite temperature observations and the surface sensor derived value. However, it is difficult to understand why the satellite values are systematically higher than the flux tower observations in this environment. In trying to solve this problem, it was realized that there are no satisfactory models for interaction between long wave radiation and this type of canopy.

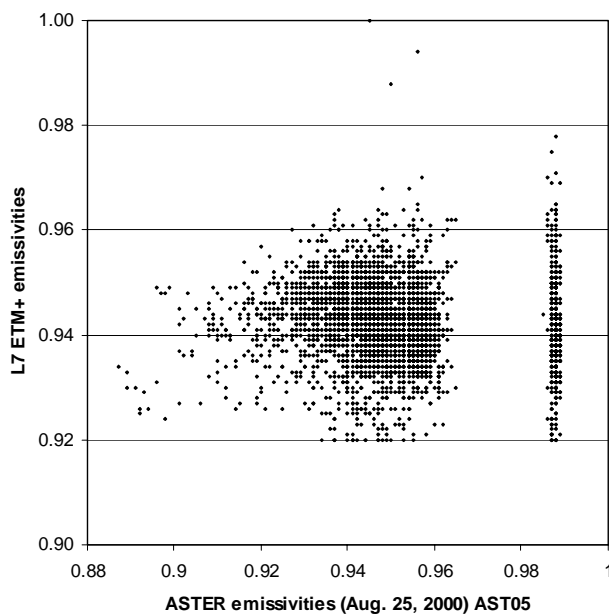


**Figure 4** Emissivities of the Aster image of Aug. 25, 2000 (product AST05) against the emissivities determined as a function of the NDVI<sup>24</sup>.

The results summarized in Table 2 underline this: The temperatures calculated with  $L_{\text{sens}} = \epsilon \sigma T_0^4$  agree better with the satellite values than the conceptually more plausible  $L_{\text{sens}} = \epsilon \sigma T_0^4 - (1 - \epsilon) L_{\downarrow}$ . With respect to the plethora of available energy balance models, it appears that models, which take into account surface-canopy radiation interactions through multi-layered approaches, are better equipped to deal with the difficulties in this terrain than the single layer models<sup>4</sup>.

Another problem in the analysis lies in the complicated nature of the input parameters required to resolve the atmospheric corrections in the radiative transfer problem. MODTRAN4 ideally requires layered atmospheric information with respect to pressure, temperature, water vapour, ozone, etc. This information comes from soundings by weather balloons or from satellite sensors. However, there is a clear need for simpler and more transparent handling of



the input parameters. The organization of such databases as the collection of NVAP Langley water vapor data is a step in the right direction, since TIR transmissivity clearly depends on atmospheric water vapor content.

With regard to the second issue, it is clear that emissivity-NDVI relations may work in certain environments and under specific climatic and environmental conditions, but they do not appear to be generally valid in any environment. The low correlation between results obtained in the independent application of the two methods shows that significant in-scene temperature differences may result. Energy balance modeling should employ them cautiously therefore.

## REFERENCES

1. Kustas, W.P., Humes, K.S., Norman, J.M. and M.S. Moran. "Single and Dual Source Modeling of Energy Fluxes with Radiometric Surface Temperature". *Journal of Applied Meteorology*, **35**, 110-121, 1996.
2. Bastiaanssen, W.G.M., Menenti, M., Feddes, R.A. and Holtslag, A.A.M. "A remote sensing surface energy balance algorithm for land (SEBAL) 1. Formulation". *Journal of Hydrology*, **212-213**, 198-212, 1998.
3. Su, Z. "The Surface Energy Balance System (SEBS) for estimation of turbulent fluxes". *Hydrology and Earth System Sciences*, **6(1)**, 85-99, 2002.
4. Timmermans, W.J., Gieske, A.S. , Wolski, P., Arneth, A. and G.N. Parodi. "Determination of water and heat fluxes with MODIS imagery – Maun, Botswana". *SPIE Proceedings Barcelona*, 2003.
5. Veenendaal, E.M., Kolle, O., and J. Lloyd. "Seasonal variation in energy fluxes and carbon dioxide exchange for a broad-leaved savanna (Mopane Woodland)". *Global Change Biology*, 2003 (in press).
6. Kealy, P.S. and S.J. Hook. "Separating temperature and emissivity in thermal infrared multispectral scanner data: Implications for recovering land surface temperatures". *IEEE Transactions on Geoscience and Remote Sensing*, **Vol 31, 6**, 1155-1164, 1993.
7. Schmutge, T., French, A., Ritchie, J., Rango, A. and H. Pelgrum. "Temperature and emissivity separation from multispectral thermal infrared observations". *Remote Sensing of Environment*, **79**, 189-198, 2002.
8. Gillespie, A., Rokugawa, S., Matsunaga, T., Cothorn, J.S., Hook, S. and A.B. Kahle. "A Temperature and Emissivity Separation Algorithm for Advanced Spaceborne Thermal Emission and Reflection Radiometer (ASTER) Images". *IEEE Transactions on Geoscience and Remote Sensing*, **Vol 36, 4**, 1113-1126, 1998.
9. Berk A., Anderson, G.P., Bernstein, L.S., Acharya, P.K., Dothe, H., Matthew, M.W., Adler-Golden, Chetwynd, J.H., Richtsmeier, S.C., Pukall, B. Allred, C.L., Jeong, L.S. and M.L. Hoke." MODTRAN4 Radiative Transfer Modeling for Atmospheric Correction". *SPIE Proceedings, Optical Spectroscopic Techniques and Instrumentation for Atmospheric and Space Research III*, **Volume 3756**, 1999.
10. Hook, S.J., Gabell, A.R., Green A.A. and P.S. Kealy. A comparison of techniques for extracting emissivity information from thermal infrared data for geologic studies. *Remote Sensing of Environment*, **Vol. 42**, 123-135, 1992.
11. Li, Z-L., Becker, F., Stoll, M.P. and Z. Wan. "Evaluation of Six Methods for extracting Relative Emissivity Spectra from Thermal Infrared Images". *Remote Sensing of the Environment*, **69**, 197-214, 1999.
12. Liang, S. "An Optimization Algorithm for Separating Land Surface Temperature and Emissivity from Multispectral Thermal Infrared Imagery". *IEEE Transactions on Geoscience and Remote Sensing*, **39(2)**, 264-274, 2001.

13. Schmugge, T., Hook, S.J. and C. Coll. "Recovering Surface Temperature and Emissivity from Thermal Infrared Multispectral Data". *Remote Sensing of Environment*, **65**, 121-131, 1998.
14. Ogawa, K., Schmugge, T., and F. Jacob, F. "Estimation of land surface window (8-12 $\mu$ m) emissivity from multispectral thermal infrared remote sensing – A case study in a part of Sahara Desert". *Geophysical Research Letters*, **30**, (2003, in press).
15. Buongiorno, M.F., Realmuto, V.J., and F. Doumaz. "Recovery of spectral emissivity from Thermal Infrared Multispectral Scanner imagery acquired over a mountainous terrain: A Case Study from Mount Etna Sicily". *Remote Sensing of Environment*, **79**, 123-133, 2002.
16. Hernandez-Baquero, E.D. and J.R. Schott. "Atmospheric compensation for surface temperature and emissivity separation". *SPIE 14<sup>th</sup> Annual International Symposium, Aerosense*, 24-28 April 2000, Orlando, Florida, USA, 2000.
17. Norman, J.M. and F. Becker. "Terminology in thermal infrared remote sensing of natural surfaces". *Agricultural and Forest Meteorology*, **77**, 153-166, 1995.
18. Qin, Z., Karnieli, A. and P. Berliner. "A mono-window algorithm for retrieving land surface temperature from Landsat TM data and its application to the Israel-Egypt border region". *International Journal of Remote Sensing*, **22 (18)**, 3719-3746, 2001.
19. Wukelic, G.E., Gibbons, D.E., Martucci, L.M. and H.P. Foote. "Radiometric Calibration of Landsat Thematic Mapper Thermal Band". *Remote Sensing of Environment*, **28**, 339-347, 1989.
20. Carlson, T.N., Taconet, O., Vidal, A., Gillies, R.R., Olioso, A. and K. Humes. "An overview of the workshop on thermal remote sensing held at La Londe les Maures, France, September 20-24, 1993". *Agricultural and Forest Meteorology*, **77**, 141-151, 1995.
21. Lagouarde, J.P., Kerr, Y.H., and Y. Brunet. "An experimental study of angular effects on surface temperature for various plant canopies and bare soils". *Agricultural and Forest Meteorology*, **77**, 167-190, 1995.
22. Palluconi, F., Hoover, G., Alley, R., Jentoft-Nilsen, M. and T. Thompson. "An Atmospheric Correction Method for ASTER Thermal Radiometry over Land". ASTER Standard Data Product AST09, JPL, Pasadena, CA, USA, 1999.
23. Thome, K., Arai, K., Hook, S., Kieffer, H., Lang, H. Matsunaga, T., Ono, A., Palluconi, F., Sakuma, H., Slater, P., Takashima, T., Tonooka, H., Tsuchida, S., Welch, R.M. and E. Zalewski. "ASTER Preflight and Inflight Calibration and the Validation of Level 2 Products". *IEEE Transactions on Geoscience and Remote Sensing*, **36 (4)**, 1161-1172, 1998.
24. Van de Griend, A.A. and M. Owe. "On the relationship between thermal emissivity and the normalized difference vegetation index for natural surfaces. *International Journal of Remote Sensing*, **14(6)**, 119-131.